Marine Research
of the National Academy of Marine Research
ISSN: 2709-6629 (Vol.4 Iss.2)
GPN: 2011200033

DOI: http://dx.doi.org/10.29677/MR.202412_4(2).0001
2024, 4(2), 1-16

Investigation of the Performance of Piezoelectric Wave Energy Harvesters Using a Buoy Design

Shao-En Chen [1] Yu-Xiang Hsu [1] Ray-Yeng Yang [2] Chia-Che Wu [1*]

[1] *Department of Mechanical Engineering, National Chung Hsing University, Taichung, Taiwan*
[2] *Department of Hydraulic and Ocean Engineering, National Cheng-Kung University, Tainan, Taiwan*

ABSTRACT

This study proposes a piezoelectric wave energy harvester (PWEH) that integrates a unidirectional rotation mechanism with piezoelectric power generation components using buoys with added mass. By formulating the structural configuration of the buoy and augmenting the mass of the buoy, the inherent frequency of the buoy is modified to synchronize with the oscillation of the waves. A rotating cam is employed to trigger vibrations in the piezoelectric cantilever beam, resulting in a consistent generation of electrical energy via the piezoelectric phenomenon. The apparatus comprises a buoy, a unidirectional rotation mechanism, and components for piezoelectric power generation. The piezoelectric power generation element, which serves as the primary power generation module within the apparatus, utilizes a compound cantilever beam configuration consisting of a brass base and lead zirconate titanate (PZT) material. Performance measurement of the PWEH was conducted using the wave flume test at the Tainan Hydraulics Laboratory, National Cheng Kung University (THL, NCKU), Taiwan. The device exhibited optimal performance at various sizes and masses of the buoys. The measured Response Amplitude Operator (RAO) values were all greater than 0.55, with a maximum value of 1.209. For Buoy B-3 under wave conditions of a 1-s wave period and 75-mm wave amplitude, the average output shaft speed was 4.602 rad/s, and the open-circuit output voltage was 5.01 V. Through rectification and filtering circuits connected to a load impedance of 10 kΩ and a bypass capacitor of 33 nF, the filtered output root mean square voltage was measured at 4.29 V, with an average electrical power of 1.840 mW.

Keywords: wave energy, piezoelectric cantilever, piezoelectric wave energy harvester, unidirectional rotation mechanism.

* Corresponding author, e-mail: josephwu@dragon.nchu.edu.tw (C.-C. Wu).

Received June 29, 2024, accepted September 11, 2024.

1 INTRODUCTION

Located in a low-latitude zone and entirely surrounded by the sea, Taiwan has ideal geographical conditions for harnessing wave energy. Estimates suggest that the wave energy density in nearby seas ranges from 10 to 20 kW/m². Furthermore, the Ministry of Economic Affairs' feed-in tariff for renewable energy in 2023 shows that offshore wind power is priced at NT$4.51 per kilowatt-hour, while ocean energy generation is priced at NT$7.32 per kilowatt-hour, indicating a significant pricing advantage for ocean energy. Wave energy converters (WECs) are essential for converting wave energy into electricity. These devices use buoys to capture wave motion energy and employ mechanical mechanisms to drive power generation systems. In this way, WECs transform wave energy into mechanical energy, which is then converted into electricity. Developing wave energy technology not only helps address energy crises but also contributes to reducing environmental impact.

Recently, the use of piezoelectric materials in wave energy extraction technologies has attracted significant interest. Piezoelectric energy harvesters are a type of direct drive system that can directly convert the strain energy of materials into electricity through the positive piezoelectric effect, eliminating the need for intermediate mechanisms (Mutsuda et al., 2017a). Integrating piezoelectric materials into wave energy extraction has led to the development of piezoelectric wave energy harvesting techniques. These techniques use buoys and mechanical mechanisms to convert the kinetic energy of waves into mechanical energy first. Then, the positive piezoelectric effect in the materials efficiently transforms this mechanical energy into electricity. Despite facing numerous challenges, such as unpredictable weather, fluctuating wave frequencies, and harsh marine environments, researchers are increasingly interested in exploring piezoelectric materials for wave energy extraction due to their relatively lower costs, ease of maintenance, and versatility.

Liu et al. (2023) offered a comprehensively reviewed exploration of the cutting-edge developments and inherent challenges within the realm of ocean wave energy harvesting technologies (Liu et al., 2023). Their work delves into the theoretical underpinnings of sea waves, dissects the diverse array of ocean wave energy harvesters, and meticulously examines the methodologies employed for transferring wave energy. The study underscores the paramount influence of architectural design and component selection on the output performance of wave energy harvesters. The rapid evolution of wave energy harvesting technologies signals a promising outlook for this field, suggesting that ongoing research and development endeavors will continue to refine and enhance these systems. Barua et al. (2024) spotlit significant advances in ocean wave energy harvesting (EH) technologies, centering on various types such as triboelectric, piezoelectric, and electromagnetic harvesters (Barua et al., 2024). A comprehensive comparison of the output performance of different energy harvesting devices has been presented. This comparison illuminates how architectural design and component selection exert a significant impact on the efficiency and effectiveness of these devices. In a comprehensive review, Kargar et al. (2022) cataloged 85 designs of piezoelectric energy harvesters for marine applications documented in recent literature. These designs encompass various configurations, including cantilever beams, thin films, and patch types. The catalog also details material selection, coupling modes, deployment locations, and power output ranges for each design (Kargar et al., 2022). Xie et al. (2014) proposed a plate-type structure for piezoelectric wave energy harvesting. This design effectively captures the transverse wave motion of water particles to generate electricity, achieving a root mean square power output of up to 30 W (Xie et al., 2014). Mutsuda et al. (2017b) developed an innovative piezoelectric wave power generation device. Their design embeds flexible piezoelectric components within an experimental tank. Using a wave generator to create periodic waves and strain the piezoelectric components, this setup leverages the electromechanical conversion properties of the materials for power generation (Mutsuda et al., 2017b).

Marine Research of the National Academy of Marine Research
DOI: 10.29677/MR.202412_4(2).0001

Piezoelectric power generation components come in two main designs: non-contact and contact. Non-contact designs use electromagnetic coils for induction, creating forces that vibrate the piezoelectric material and generate electricity. In contrast, contact designs rely on mechanical means to vibrate and deform the piezoelectric material for electricity generation. The cantilever beam structure is a popular choice for contact designs because its natural frequency can be adjusted by modifying its length and thickness. By tailoring the dimensions of the piezoelectric cantilever beam to resonate with the environmental vibration frequency, the design can achieve greater deformation during operation, leading to increased electricity generation. Optimal power output is achieved through circuit design that matches the internal impedance of the component with the external impedance of the circuit. For example, Pradeesh et al. (2019) demonstrated impedance matching by adjusting the distance between the piezoelectric material and the fixed end of the cantilever beam (Pradeesh et al., 2019).

The design of buoys used in wave energy harvesters plays a critical role in maximizing energy extraction efficiency. During the design phase, careful consideration of buoy shape, size, and weight is crucial for ensuring optimal performance of the wave energy converter (WEC) under various wave conditions. Sergiienko et al. (2017) evaluated the performance of different buoy shapes (spheres, cylinders, ellipsoids, and tapered cylinders) within WECs, finding that cylindrical buoys were the most effective (Sergiienko et al., 2017). Zhang et al. (2022) optimized the shape and structural parameters of buoys used in point absorber WECs, highlighting the positive impact of increasing buoy width on power capture and bandwidth. However, increasing buoy draft can improve maximum power output but may decrease the resonance period (Zhang et al., 2022). Azam et al. (2022) introduced innovative buoy geometries for wave energy harvesting in both regular and irregular waves. They analyzed the buoys using ANSYS AQWA software to assess the effects of shape variations on power output and efficiency (Azam et al., 2022). Tao et al. (2021) proposed three key design principles for buoys: 1) matching the buoy's frequency to the wave frequency with a broad resonance bandwidth, 2) maintaining stability to prevent capsizing under wave action and ensuring post-wave stability, and 3) considering cost-effectiveness, as buoy cost typically increases with weight. They also provided design guidelines, resonance conditions, and discussed the optimal diameter range for cylindrical buoys, which is typically between 5% and 10% of the wavelength. Experimental results further confirmed the significant influence of buoy radius and draft on energy extraction (Tao et al., 2021). In our previously published research, we derived a mathematical model of the composite piezoelectric cantilever beam utilizing Euler-Bernoulli beam theory (Chen et al., 2021). Additionally, we developed multiphysics system integration and modeling methods, encompassing hydrodynamic, kinematic, and electromechanical models (Chen et al., 2023).

This study addresses the aforementioned challenges by developing a piezoelectric wave energy harvester (PWEH) that utilizes the positive piezoelectric effect to generate electricity. In order to enhance the efficiency of wave energy extraction, the design of the buoy has emphasis placed on the optimization of weight by added mass to achieve improved stability while tracking waves. Additionally, the natural resonance frequency was adjusted to match wave motion, further increasing extraction efficiency. To convert low-frequency wave oscillations into higher-frequency unidirectional rotation, a novel mechanism using one-way bearings was implemented. A cam on the spindle then induced deformation in the piezoelectric cantilever beam, generating electricity through a plucking motion. This design mitigated damage to the piezoelectric elements caused by unstable impact forces from repeated rotations and reduces the instantaneous decay of rotational speed. This ensured stable driving of the piezoelectric components, leading to consistent electrical energy output. Finally, a flywheel on the output shaft increased the moment of inertia of the rotating system, stabilizing its rotational speed and minimizing fluctuations in output shaft speed. To validate the power generation performance of the PWEH, the device underwent testing in the wave flume at the Tainan Hydraulics Laboratory, National Cheng Kung University (THL, NCKU), Taiwan.

DOI: 10.29677/MR.202412_4(2).0001

2 CONCEPTUAL DESIGN AND RESEARCH METHOD

2.1 Piezoelectric Wave Energy Harvester

The piezoelectric wave energy harvester (PWEH) developed in this study consists of three main components, as illustrated in Figure 1: the floating part, the unidirectional rotation mechanism, and the piezoelectric power generation components. Comprised of a buoy, fixation plate, and two linear slide sets, the floating part absorbs vertical wave motion and converts it into mechanical kinetic energy. The fixation plate connects the buoy to the linear slides, constraining the buoy's movement to a single vertical direction. The unidirectional rotation mechanism utilizes two sets of racks driven by the linear slides. These racks follow the buoy's vertical motion, translating it into linear movement that drives two gear sets on the same output shaft. Two one-way bearings installed between them ensure that the output shaft generates unidirectional rotation. Furthermore, a flywheel mounted on the output shaft increases the system's rotational inertia, reducing fluctuations in rotational speed and enhancing the mechanism's stability. Finally, a cam on the output shaft plucks the free end of the piezoelectric cantilever beams, directly applying force to the piezoelectric component and inducing deformation to generate electricity via the positive piezoelectric effect.

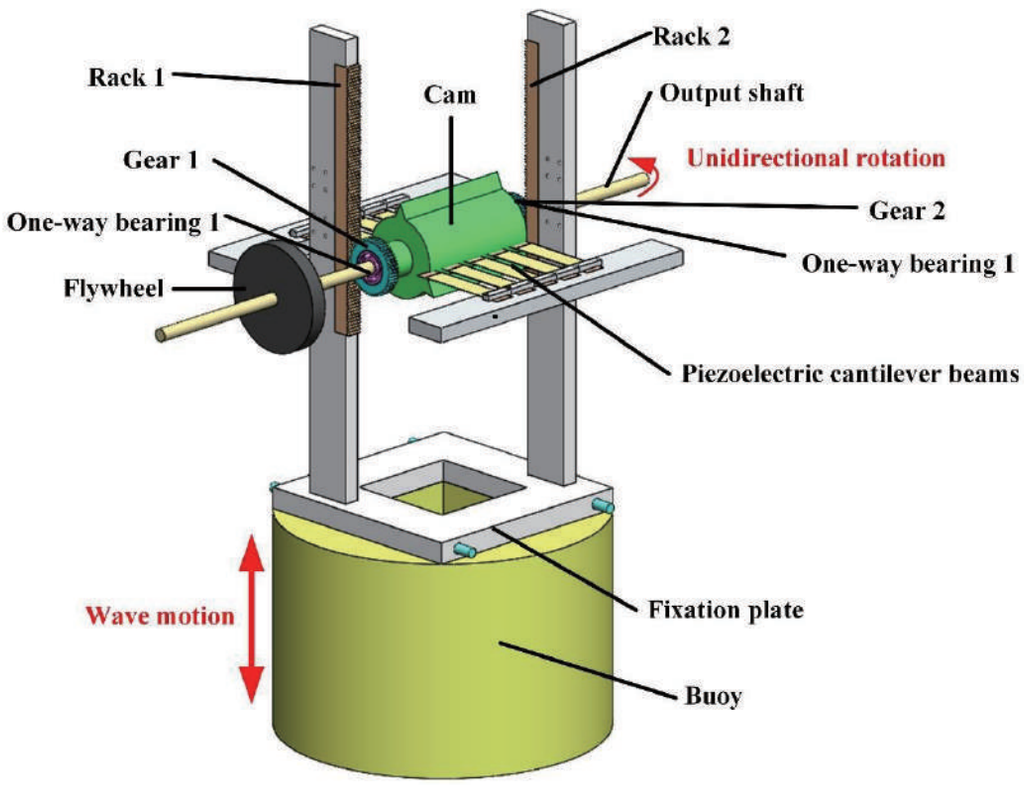

Figure 1. Schematic diagram of composite piezoelectric/electromagnetic wave energy harvester.

Marine Research of the National Academy of Marine Research
DOI: 10.29677/MR.202412_4(2).0001

2.2 Design and Analysis of Piezoelectric Power Generation Components

This study utilizes a composite cantilever beam structure for the piezoelectric power generation component. The beam comprises a brass substrate layer, a piezoelectric layer of lead zirconate titanate (PZT), and top and bottom silver electrode layers. To maximize the positive piezoelectric effect, the thickness of each layer was designed based on the neutral axis position. The transformed-section method ensures the neutral axis resides between the substrate layers, inducing greater stress in the PZT layer and maximizing energy generation. Material strength and natural frequency were also considered during design. Careful design was crucial for these brittle materials to prevent stress-induced damage and component failure. Additionally, the structure's natural frequency was tailored to match the operating frequency, enhancing the positive piezoelectric effect during resonance.

Finite element software (ANSYS) was used to analyze the composite cantilever beam's strength and modal characteristics, guiding the design of its geometric dimensions (length and width). To ensure the piezo electric component could deform under applied force without exceeding its allowable stress and to achieve resonance for maximized energy generation, meticulous design considerations were employed. Calculations determined the maximum cam force to be 3.049 N. The tensile strength of PZT was reported to be 140.4 MPa (Anton et al., 2012). A safety factor of 1.4 was incorporated during design, followed by simulation analysis. The geometric design of the piezoelectric cantilever beam (detailed in Figure 2 and Table 1) was then optimized. The analysis revealed a maximum stress value of 100.14 MPa and a first-mode natural frequency of 83.6 Hz for the structure.

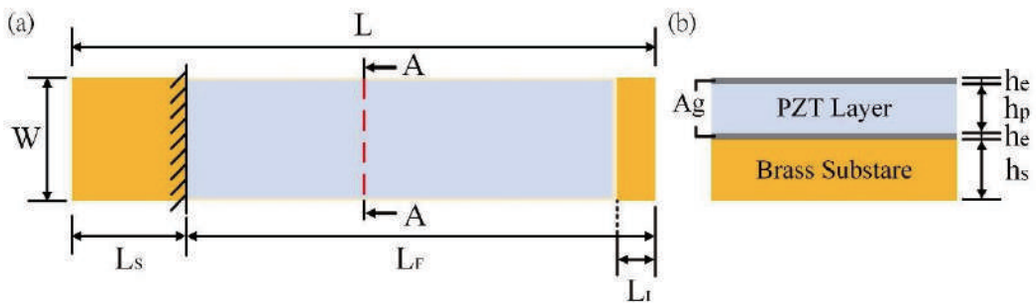

Figure 2. Geometric design illustration of the piezoelectric composite cantilever beam. (a) Geometric dimensions; (b) A-A cross-section.

Table 1. Geometric dimension parameters of the piezoelectric composite cantilever beam.

Geometric Parameter	Symbol	Value (Unit)
Length	L	95 mm
Width	W	20 mm
Length of fixed end	L_S	20 mm
Length of free end	L_F	75 mm
The length of the plucking area	L_I	5 mm
Thickness of substrate layer	h_S	400 μm
Thickness of PZT layer	h_P	400 μm
Thickness of electrode layer	h_E	2 μm
Area of electrode layer (length × width)		69 mm × 19 mm

DOI: 10.29677/MR.202412_4(2).0001

This study utilizes piezoelectric elements to generate electrical power. When a cam plucks the piezoelectric cantilever beams, they deform and produce AC voltage. To store this energy, a rectifier can be used to convert the AC voltage to DC. While the bridge rectifier circuit is a common choice, its output is a pulsating DC voltage, not a smooth DC voltage. Since most components malfunction under pulsating voltage, a smoothing capacitor and load resistor are typically added to the bridge rectifier's output for filtering (Figure 3). This combined rectification and filtering process transforms the AC output from the piezoelectric elements into a stable DC voltage suitable for powering other components.

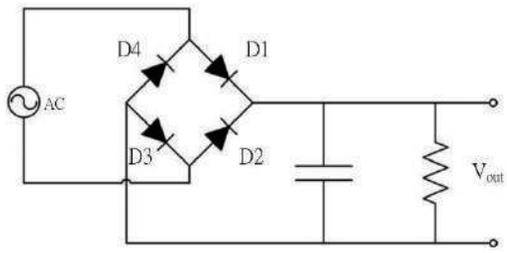

Figure 3. Schematic diagram of bridge rectifier and filter circuit.

2.3 Analysis and Design of Buoys' Structures and Load Considerations

Buoys play a crucial role in wave energy converter (WEC) design. To maximize wave energy capture and power generation, the buoy shape, size, and weight across various wave conditions must be considered in WEC design for optimal performance. Azam et al. (2022) suggests that increasing buoy width significantly impacts capture power and bandwidth, thereby enhancing captured wave energy and power generation (Azam et al., 2022). However, increasing buoy draft can raise maximum power but may lower the resonance period. This study proposes three cylindrical buoy design schemes for WECs, as shown in Figure 4. All design parameters of the buoys, including dimensions, drafts, and total weights, are summarized in Table 2. By comprehensively considering the effects of buoy width and draft on capture power, bandwidth, and resonance period, optimal performance under diverse wave conditions can be ensured for WEC buoy design.

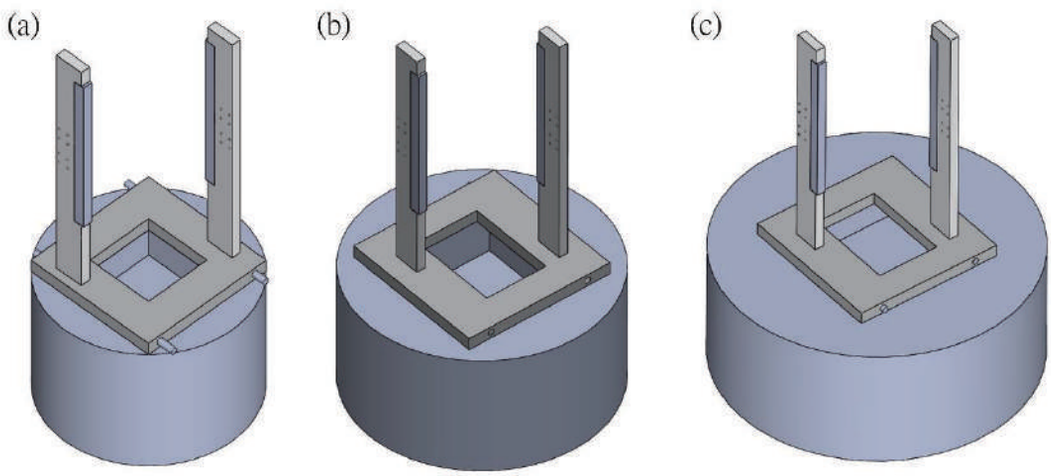

Figure 4. Schematic diagram of buoy design with different diameters. (a) Buoy A with a diameter of 300mm; (b) Buoy B with a diameter of 400mm; (c) Buoy C with a diameter of 500mm.

DOI: 10.29677/MR.202412_4(2).0001

Table 2. Parameter table for buoy design.

Buoy Number	Diameter (mm)	High (mm)	Draft (mm)	Total mass (kg)
A-1	300	200	15	1.03
A-2	300	200	46	3.30
A-3	300	200	63	4.40
B-1	400	200	15	1.70
B-2	400	200	53	7.10
B-3	400	200	77	9.60
C-1	500	200	08	1.94
C-2	500	200	53	11.14
C-3	500	200	79	15.50

2.4 Simulation of Response Amplitude Operator of Buoys

To evaluate the influence of design parameters on piezoelectric wave energy harvester (PWEH) performance, this study designed three buoys with varying sizes and assigned three different weights to each. ANSYS AQWA software was used to simulate the buoys' responses to wave motion. Nine buoy configurations were analyzed in ANSYS AQWA for hydrodynamic performance. The response amplitude operator (RAO) of the buoys under regular waves was calculated, and its impact on PWEH performance was assessed.

The simulation results for the three buoys with varying drafts are presented in Figures 5 to 7. These results demonstrate that increasing a buoy's draft, achieved by increasing its weight, leads to a longer resonance period and a more pronounced resonance phenomenon. For instance, in Figure 5, Buoy A exhibits a simulated resonance period of 0.74 seconds and a RAO value of 1.448 when its draft is 46 mm. When the draft is increased to 63 mm, the simulated resonance period becomes 0.77 seconds, and the RAO value increases to 1.883. Similar trends are observed in Figures 6 and 7 for Buoys B and C, respectively. Analysis of the simulations reveals a positive correlation between a buoy's draft and both the resonance period and the RAO value. Consequently, increasing a buoy's draft can enhance the resonance of its motion, leading to a higher RAO and enabling the PWEH to capture more wave energy for improved power generation performance.

Marine Research of the National Academy of Marine Research
DOI: 10.29677/MR.202412_4(2).0001

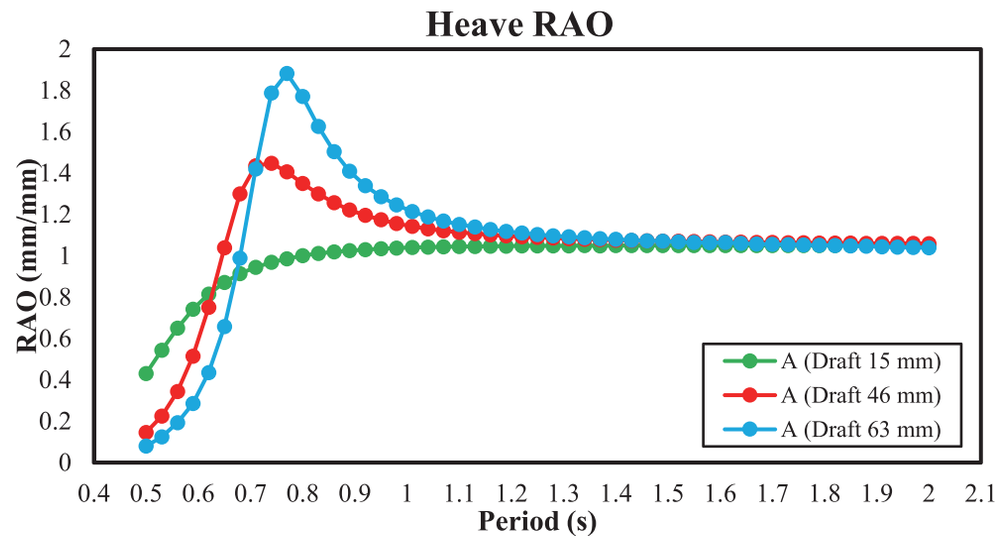

Figure 5. RAO simulation results of Buoy A.

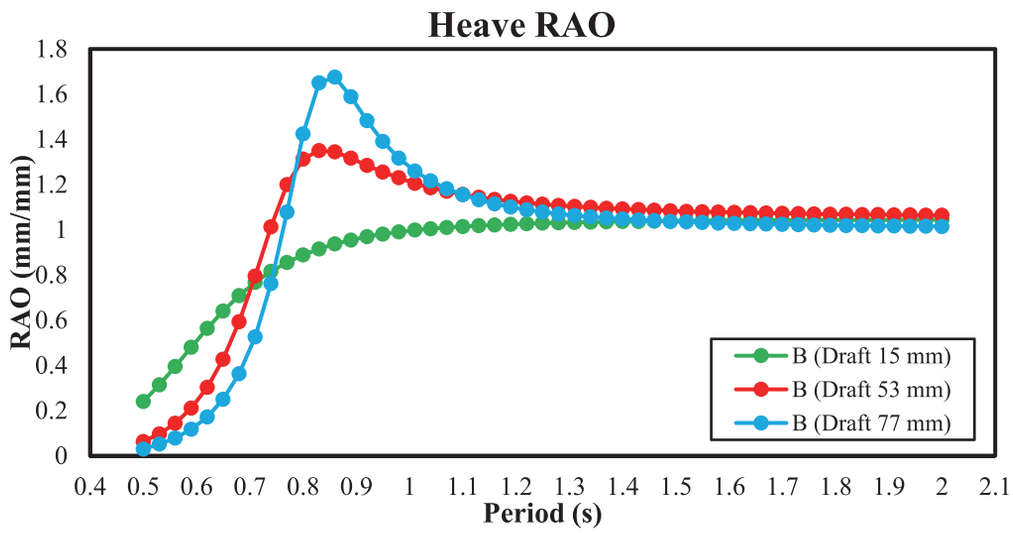

Figure 6. RAO simulation results of Buoy B.

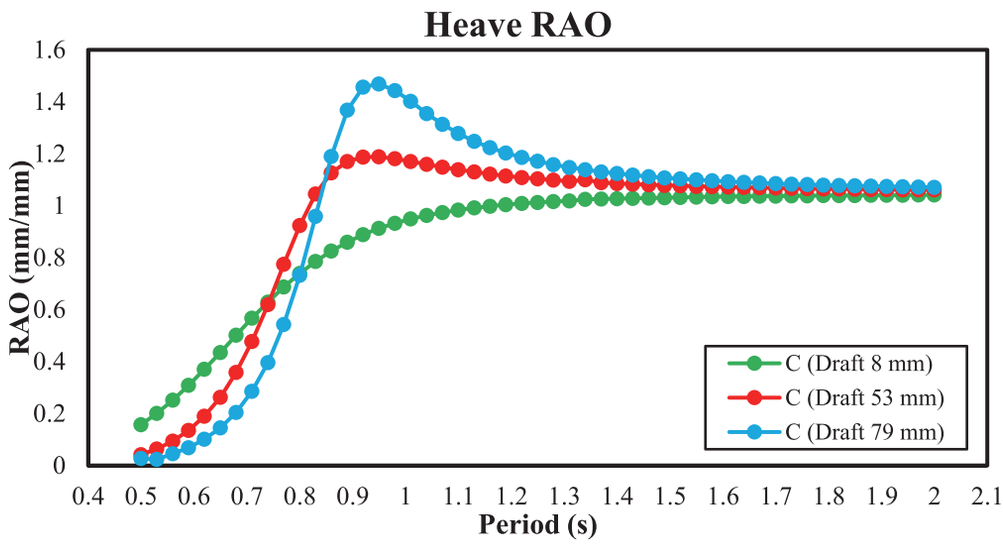

Figure 7. RAO simulation results of Buoy C.

Marine Research of the National Academy of Marine Research
DOI: 10.29677/MR.202412_4(2).0001

2.5 Experimental Setup

In collaboration with the Tainan Hydraulics Laboratory, National Cheng Kung University (THL, NCKU), Taiwan, this study conducted practical performance tests of the PWEH within the experimental wave tank facility. A wave generator was used to create waves with specific periods and heights, allowing measurement of the harvester's power generation efficiency under various wave conditions. The experimental wave parameters, detailed in Table 3, included three wave periods and two wave heights, resulting in a total of six test configurations. The PWEH was then subjected to these six configurations, and its power generation efficiency was measured.

Table 3. Wave-period and wave-height-parameter generated by the wave machine.

Wave Period (s)	1.0	1.5	2.0
Wave height (100 mm)	Case1	Case2	Case3
Wave height (150 mm)	Case4	Case5	Case6

Figure 8 illustrates the overall experimental setup. The capacitive wave gauge was positioned 9 meters from the wave generator, while the PWEH was located 14 meters away. After the wave generator created waves, the wave gauge installed in the tank measured the actual wave height and period. Once the harvester stabilized its operation under wave action, a video recorder captured the motion trajectory of the buoy for subsequent image analysis, allowing for the determination of the buoys' actual displacement. Additionally, an encoder measured the rotational speed of the output shaft. Finally, the power signal generated by the piezoelectric component was rectified and filtered using a bridge rectifier circuit. An oscilloscope then observed and stored the experimental data.

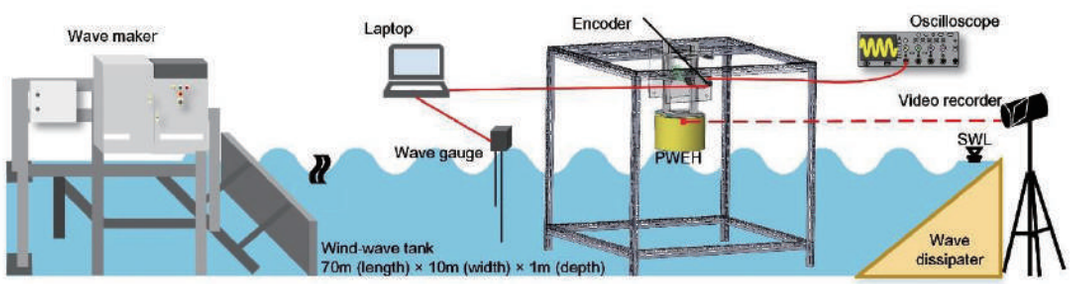

Figure 8. Schematic diagram of experimental setup.

Marine Research of the National Academy of Marine Research
DOI: 10.29677/MR.202412_4(2).0001

3 RESULTS AND DISCUSSION

3.1 Displacement Results of Buoys

This study utilized a photographic method to record the vertical displacement of nine buoy configurations. MATLAB was employed to convert pixel position changes into actual buoy displacements. The zero-upcrossing method was then used to calculate the average peak displacement (oscillation amplitude) of the buoy in the vertical direction. In the experiment, a wave gauge was also used to measure the amplitude of the actual wave, and the zero-upcrossing method was also used to calculate the average amplitude of the wave. Table 4 presents the measured average wave amplitude and the average displacement of the buoy motion under stable waves for the first 30 seconds after wave generation for all buoy configurations under six wave generation parameters. The results indicate that all buoy configurations, except B-2 and C-2, exhibit larger displacements at a period of 1.5 seconds (experimental cases 02 and 05) regardless of wave height. This suggests that resonance occurs near a period of 1.5 seconds, leading to larger displacement amplitudes.

Table 4. Table of average oscillation amplitude results of buoys and average measured wave amplitude results in wave experiments.

Buoy Number	Average oscillation amplitude of the buoys (mm) / Average measured amplitude of waves (mm)					
	Case 01	Case 02	Case 03	Case 04	Case 05	Case 06
A-1	40.23 / 58.56	53.00 / 49.03	49.72 / 52.73	54.38 / 83.92	60.06 / 82.50	51.33 / 75.94
A-2	39.14 / 58.59	50.93 / 49.06	47.93 / 52.73	61.43 / 83.81	75.68 / 82.53	68.37 / 75.88
A-3	30.18 / 58.61	48.42 / 49.05	48.31 / 52.74	65.28 / 83.9	77.51 / 82.46	69.87 / 75.86
B-1	44.80 / 58.56	54.38 / 49.03	49.64 / 52.75	74.14 / 83.86	75.89 / 82.49	66.21 / 75.92
B-2	39.87 / 58.55	55.24 / 49.06	52.08 / 52.76	80.10 / 85.76	70.23 / 73.00	71.99 / 75.86
B-3	44.15 / 58.55	52.31 / 49.03	51.41 / 52.73	55.79 / 83.89	76.59 / 82.53	66.70 / 75.88
C-1	49.01 / 58.55	58.32 / 49.05	52.63 / 52.73	72.12 / 83.87	76.13 / 79.46	74.96 / 79.40
C-2	40.10 / 58.54	59.32 / 49.07	51.44 / 52.75	76.54 / 86.97	74.85 / 79.37	73.90 / 81.48
C-3	39.53 / 58.87	47.79 / 49.07	46.36 / 52.75	49.40 / 83.87	71.93 / 76.93	70.47 / 75.94

DOI: 10.29677/MR.202412_4(2).0001

Following analysis of the measured buoy displacements and wave amplitudes, RAO values were calculated for all buoys under various wave parameters (Table 5). The RAO values are the ratio of the vertical displacement of the buoy to the amplitude of the wave. These results exhibit similar trends across the nine buoy configurations. When waves do not induce resonance in a buoy system, shorter wave periods correspond to shorter wavelengths according to physical principles. In this scenario, the buoy behaves as a large structure relative to the wave length. Consequently, waves are easily shielded and cannot penetrate the buoy, hindering its ability to follow wave motion. This explains the observed decrease in RAO values with decreasing wave periods. Notably, Buoys A, B, and C achieved their maximum RAO values at a period of 1.5 seconds, with Buoy C-2 exhibiting the highest value (1.209). This suggests that the wave motions at this period align closely with the buoys' resonance periods, leading to a more pronounced resonance effect. This effect allows the buoys to experience larger amplitudes, resulting in higher RAO values.

Table 5. Table of RAO values of buoys in wave experiments.

Buoy Number	RAO value of the buoys					
	Case 01	Case 02	Case 03	Case 04	Case 05	Case 06
A-1	0.687	1.081	0.943	0.648	0.728	0.676
A-2	0.668	1.038	0.909	0.733	0.917	0.901
A-3	0.515	0.987	0.916	0.778	0.94	0.921
B-1	0.765	1.109	0.941	0.884	0.92	0.872
B-2	0.681	1.126	0.987	0.934	0.962	0.949
B-3	0.754	1.067	0.975	0.665	0.928	0.879
C-1	0.837	1.189	0.998	0.860	0.958	0.944
C-2	0.685	1.209	0.975	0.880	0.943	0.907
C-3	0.675	0.974	0.879	0.589	0.935	0.928

Comparing the RAO simulation results from Subsection 2.4 with the experimental results in Table 5, we observe discrepancies in resonance period and amplitude values. The inconsistencies between the measured heave amplitudes and the AQWA predictions is a valuable finding. One possible reason for these inconsistent results is the viscous effects produced by the buoy as it moves through the water tank environment. While powerful, the AQWA simulation software may have inherent limitations in representing certain aspects of buoy dynamics, particularly when dealing with complex viscous effects. Moreover, the AQWA simulation primarily focuses on the hydrodynamic analysis of a single buoy body. However, our actual water tank experiment involves assembled mechanisms and power generation components, altering the overall mechanical mass-spring-damping system. This deviation from a single floating body likely contributed to the differences between the simulation results and experimental data. In the future, we will conduct a series of controlled experiments under various conditions to systematically validate the numerical model against experimental data.

DOI: 10.29677/MR.202412_4(2).0001

3.2 Angular Velocity Measurement Results for the Output Shaft

This study's PWEH utilizes buoys to capture wave energy. A mechanical design converts the buoys' vertical motion into unidirectional rotational motion of the output shaft. An encoder measures and records the output shaft's angular speed. Table 6 summarizes the average angular speeds for the nine buoy configurations under wave motion, based on experiments with various wave conditions. The results show that the PWEH achieves higher average angular speeds at a wave height of 150 mm and a period of 1 second. This can be attributed to two factors: the rapid water level changes caused by the shorter wave period and the larger buoy displacements induced by the higher wave height. Both factors contribute to the increased final output angular speed. Furthermore, inducing resonance between the buoy and wave motion could further enhance the average angular speed by enabling the buoy to better follow the wave motion and drive the output shaft rotation through the up-and-down displacement of the rack.

Table 6. Table of average angular speed of output shaft in wave experiments.

Buoy Number	Average angular speed of output shaft (rad/s)					
	Case 01	Case 02	Case 03	Case 04	Case 05	Case 06
A-1	3.895	3.836	3.598	4.321	4.285	3.823
A-2	3.829	3.945	3.721	4.609	4.075	3.970
A-3	4.101	4.097	3.945	4.500	4.213	3.987
B-1	4.050	4.096	3.691	4.375	4.083	3.739
B-2	3.934	4.136	3.992	4.465	4.108	3.999
B-3	3.954	4.046	3.922	4.602	4.278	4.040
C-1	3.829	4.100	3.799	4.524	4.148	3.865
C-2	4.045	4.186	3.798	4.452	4.309	3.969
C-3	4.191	4.188	3.648	4.475	4.156	3.840

The results in Section 3.1 and Section 3.2 demonstrate that a higher RAO value does not necessarily correlate with a higher angular speed of the output shaft. This is because the unidirectional rotation mechanism is driven by the buoy's motion with the waves, so its rotating motion is influenced by wave amplitude and wave period. While the larger RAO result (maximum wave amplitude) is achieved at a 1.5-second wave period, a higher driving frequency at a 1-second wave period can lead to higher rotational motion of the rotating mechanism, potentially improving operating efficiency.

Marine Research of the National Academy of Marine Research
DOI: 10.29677/MR.202412_4(2).0001

3.3 Electrical Output Results of PWEH

This study investigates wave energy extraction using buoys under varying wave conditions. A mechanical mechanism converts the buoy's motion into unidirectional rotation of the output shaft. This rotation drives a cam to pluck the piezoelectric generation component, generating electrical power. The piezoelectric generation component consists of ten composite piezoelectric cantilever beams. The open-circuit output voltage was measured with an oscilloscope; these measurements are summarized in Table 7. According to wave theory, waves with shorter periods and higher heights have greater energy density. Buoys A-1, A-2, and A-3 exhibited the highest open-circuit output voltages (4.38 V, 4.63 V, and 8.76 V, respectively) under wave conditions of 1 second period and 150 mm height. Buoys B-1 and B-2 achieved the highest open-circuit output voltages (6.12 V and 8.47 V) under similar wave conditions. Similarly, Buoys C-1, C-2, and C-3 demonstrated the highest filtered output voltages (7.86 V, 6.26 V, and 5.18 V, respectively) under similar wave conditions.

Table 7. Table of open-circuit output voltages of PWEH in wave experiments.

Buoy Number	Open-circuit output voltages of PWEH (V)					
	Case 01	Case 02	Case 03	Case 04	Case 05	Case 06
A-1	3.42	2.97	2.04	4.38	4.22	2.71
A-2	3.25	3.42	2.74	4.63	4.25	3.67
A-3	5.67	8.08	7.86	8.76	8.67	4.92
B-1	5.62	5.35	4.25	6.12	5.26	4.29
B-2	7.81	5.88	5.52	8.47	8.23	5.47
B-3	6.13	4.96	4.84	5.01	3.53	3.30
C-1	3.51	3.10	2.89	7.86	7.28	6.33
C-2	4.56	3.92	3.33	6.26	5.39	4.90
C-3	4.47	4.06	3.38	5.18	4.99	4.51

This study employed a diode bridge for rectification and a capacitor for filtering. A 10 kΩ load resistor was then used to measure the output voltage. The measured results are summarized in Table 8. The trend of the filtered output voltage aligns with that of the open-circuit output voltage. Buoys A-1, A-2, and A-3 achieved the highest filtered output voltages (2.53 V, 2.61 V, and 2.57 V, respectively) under wave conditions of 150 mm height and 1 second period. Buoys B-1, B-2, and B-3 achieved the highest filtered output voltages (2.59 V, 4.06 V, and 4.29 V, respectively) under similar wave conditions. Similarly, Buoys C-1, C-2, and C-3 demonstrated the highest filtered output voltages (4.04 V, 2.74 V, and 2.90 V, respectively) under similar wave conditions. While successful filtering with a capacitor reduces the pulsating DC amplitude, resulting in a smoother output voltage, it also comes at the cost of a decrease in the output voltage.

Marine Research of the National Academy of Marine Research
DOI: 10.29677/MR.202412_4(2).0001

Table 8. Table of filtered output voltages of PWEH in wave experiments.

Buoy Number	Filtered output voltages of PWEH (V)					
	Case 01	Case 02	Case 03	Case 04	Case 05	Case 06
A-1	1.60	1.16	1.00	2.53	1.60	1.30
A-2	1.44	1.39	1.20	2.61	1.86	1.95
A-3	2.00	2.00	1.74	2.57	1.96	1.79
B-1	2.30	2.00	1.55	2.59	1.96	1.55
B-2	3.73	2.64	1.32	4.06	3.76	2.26
B-3	3.88	3.25	2.56	4.29	3.30	3.51
C-1	3.10	2.89	2.00	4.04	3.51	2.89
C-2	1.83	2.33	1.33	2.74	2.12	1.96
C-3	2.88	1.55	1.60	2.90	2.62	2.70

3.4 Average Power Outputs of PWEH

Average power output was calculated for all wave conditions using the measured filtered load resistor voltage. The results are summarized in Table 9. At a constant wave period, output power increases with increas ing wave height. Buoys A-1, A-2, and A-3 achieved the highest average output power (0.625, 0.681, and 0.660 mW, respectively) under wave conditions of 150 mm height and 1 second period. Buoys B-1, B-2, and B-3 achieved the highest average output power (0.670, 1.648, and 1.840 mW, respectively) under similar conditions. Similarly, buoys C-1, C-2, and C-3 demonstrated the highest average output power (1.632, 0.751, and 0.841 mW, respectively) under similar conditions.

Table 9. Table of average output powers of PWEH in wave experiments.

Buoy Number	Average output powers of PWEH (mW)					
	Case 01	Case 02	Case 03	Case 04	Case 05	Case 06
A-1	0.256	0.134	0.100	0.625	0.240	0.169
A-2	0.207	0.193	0.144	0.681	0.346	0.380
A-3	0.400	0.400	0.303	0.660	0.384	0.320
B-1	0.529	0.400	0.240	0.670	0.384	0.240
B-2	1.384	0.697	0.174	1.648	1.414	0.511
B-3	1.505	1.056	0.655	1.840	1.089	1.232
C-1	0.961	0.835	0.400	1.632	1.232	0.835
C-2	0.335	0.543	0.177	0.751	0.449	0.384
C-3	0.829	0.240	0.256	0.841	0.686	0.729

DOI: 10.29677/MR.202412_4(2).0001

4 CONCLUSIONS

This study investigates the design of a piezoelectric wave energy harvester (PWEH), focusing on optimizing buoy dimensions and mass to improve resonance response and capture more wave energy at deeper draft depths. The piezoelectric cantilever beams are excited by a cam, using brass as the substrate and lead zirconate titanate (PZT) blocks as the piezoelectric layer. The thicker PZT layer, compared to thin films, results in higher power generation efficiency. Three wave periods (1 second, 1.5 seconds, and 2 seconds) and two wave heights (100 millimeters and 150 millimeters) are employed as experimental parameters, with nine buoy configurations tested.

The experimental results, analyzed using Response Amplitude Operator (RAO), reveal that Buoys A, B, and C achieved their maximum RAO values at a 1.5-second period. Buoy C-2 exhibited the highest value (1.209). In terms of rotation measurements, Buoys A-1, A-2, and A-3 exhibited the highest average angular speed of the output shaft (4.321 rad/s, 4.609 rad/s, and 4.500 rad/s, respectively) under wave conditions of a 1-second period and 150-millimeter height. Similar trends were observed for Buoys B and C under the same wave conditions.

Electrical measurements showed that Buoys A-1, A-2, and A-3 exhibited the highest open-circuit output voltages (4.38 V, 4.63 V, and 8.76 V, respectively) under the same wave conditions as the rotation measurements. Buoys B-1 and B-2 achieved the highest open-circuit output voltages (6.12 V and 8.47 V) under similar conditions. Buoys C-1, C-2, and C-3 demonstrated the highest filtered output voltages (7.86 V, 6.26 V, and 5.18 V, respectively) under similar wave conditions.

Finally, the power output results showed that Buoys A-1, A-2, and A-3 achieved the highest average output power (0.625 mW, 0.681 mW, and 0.660 mW, respectively) under wave conditions of 150-millimeter height and a 1-second period. Buoys B-1, B-2, and B-3 achieved the highest average output power (0.670 mW 1.648 mW, and 1.840 mW, respectively) under similar conditions. Buoys C-1, C-2, and C-3 demonstrated the highest average output power (1.632 mW, 0.751 mW, and 0.841 mW, respectively) under similar conditions. The experiments confirm that the PWEH can generate electricity from wave motion. Increasing buoy mass enhances their wave-following ability, ultimately improving the PWEH's overall power generation efficiency. Although the scale of electrical power generated is not substantial enough for direct connection to the urban power grid, this small-scale electric energy can be directly supplied to offshore electronic facilities, making them self-sufficient and reducing maintenance and battery replacement costs. In the future, the system can be integrated with existing infrastructure, such as offshore wind farms or aquaculture farms, to harness ambient energy sources more effectively.

ACKNOWLEDGEMENTS

This research is supported (in part) by National Science Council of Taiwan under grant numbers under grant numbers MOST 110-2221-E-005-073, MOST 111-2218-E-005-011, NSTC 111-2811-E-005-015 and NSTC 112-2221-E-005-087.

DOI: 10.29677/MR.202412_4(2).0001

REFERENCES

Anton, S. R., Erturk, A., & Inman, D. J. (2012). Bending strength of piezoelectric ceramics and single crystals for multifunctional load-bearing applications. *IEEE Transactions on Ultrasonics, Ferroelectrics, and Frequency Control, 59*(6), 1085-1092. http://dx.doi.org/10.1109/TUFFC.2012.2299

Azam, A., Ahmed, A., Li, H., Tairab, A. M., Jia, C., Li, N., & Zhang, Z. (2022). Design and analysis of the optimal spinning top-shaped buoy for wave energy harvesting in low energy density seas for sustainable marine aquaculture. *Ocean Engineering, 255,* 111434. https://doi.org/10.1016/j.oceaneng.2022.111434

Barua, A., & Rasel, M. S. (2024). Advances and challenges in ocean wave energy harvesting. *Sustainable Energy Technologies and Assessments, 61,* 103599. https://doi.org/10.1016/j.seta.2023.103599

Chen, S. E., Yang, R. Y., Qiu, Z. H., & Wu, C. C. (2021). A piezoelectric wave energy harvester using plucking-driven and frequency up-conversion mechanism. *Energies, 14*(24), 8441. https://doi.org/10.3390/en14248441

Chen, S. E., Pan, F. T., Yang, R. Y., & Wu, C. C. (2023). A multi-physics system integration and modeling method for piezoelectric wave energy harvester. *Applied Energy, 349,* 121654. https://doi.org/10.1016/j.apenergy.2023.121654

Kargar, S. M., & Hao, G. (2022). An atlas of piezoelectric energy harvesters in oceanic applications. *Sensors, 22*(5), 1949. https://doi.org/10.3390/s22051949

Liu, R., He, L., Liu, X., Wang, S., Zhang, L., & Cheng, G. (2023). A review of collecting ocean wave energy based on piezoelectric energy harvester. *Sustainable Energy Technologies and Assessments, 59,* 103417. https://doi.org/10.1016/j.seta.2023.103417

Mutsuda, H., Tanaka, Y., Patel, R., Doi, Y., Moriyama, Y., & Umino, Y. (2017a). A painting type of flexible piezoelectric device for ocean energy harvesting. *Applied Ocean Research, 68*, 182-193. https://doi.org/10.1016/j.apor.2017.08.008

Mutsuda, H., Tanaka, Y., Patel, R., & Doi, Y. (2017b). Harvesting flow-induced vibration using a highly flexible piezoelectric energy device. *Applied Ocean Research, 68*, 39-52. https://doi.org/10.1016/j.apor.2017.08.004

Pradeesh, E. L., & Udhayakumar, S. (2019). Effect of placement of piezoelectric material and proof mass on the performance of piezoelectric energy harvester. *Mechanical Systems and Signal Processing, 130,* 664-676. https://doi.org/10.1016/j.ymssp.2019.05.044

Sergiienko, N. Y., Cazzolato, B. S., Ding, B., Hardy, P., & Arjomandi, M. (2017). Performance comparison of the floating and fully submerged quasi-point absorber wave energy converters. *Renewable Energy, 108*, 425-437. https://doi.org/10.1016/j.renene.2017.03.002

Tao, J., Cao, F., Dong, X., Li, D., & Shi, H. (2021). Optimized design of 3-DOF buoy wave energy converters under a specified wave energy spectrum. *Applied Ocean Research, 116,* 102885. https://doi.org/10.1016/j.apor.2021.102885

Xie, X. D., Wang, Q., & Wu, N. (2014). Energy harvesting from transverse ocean waves by a piezoelectric plate. *International Journal of Engineering Science, 81,* 41-48. https://doi.org/10.1016/j.ijengsci.2014.04.003

Zhang, B., Deng, Z., Miao, Y., Zhao, B., Wang, Q., & Zhang, K. (2022). Optimization of energy-capture performance of point-absorber wave energy converter. *International Journal of Energy Research, 46*(7), 9444-9455. https://doi.org/10.1002/er.7816